



GLOBAL JOURNAL OF SCIENCE FRONTIER RESEARCH
PHYSICS AND SPACE SCIENCE
Volume 13 Issue 7 Version 1.0 Year 2013
Type : Double Blind Peer Reviewed International Research Journal
Publisher: Global Journals Inc. (USA)
Online ISSN: 2249-4626 & Print ISSN: 0975-5896

Effect of Power Law Temperature Variation on a Vertical Conical Annular Porous Medium

By Dr. D. Prabhakar & Dr. G. Prabhakararao

Government Degree College, India

Abstract- In this chapter, we concentrate on the study of heat transfer by natural convection in a saturated porous medium with a power law temperature variation on a vertical conical annular porous medium". In this study Finite Element Method (FEM) has been used to solve the governing partial differential equations. There have been considerable interest in studying natural or buoyancy – induced flows in fluid saturated porous media adjacent to surfaces in recent years. This interest stems from numerous possible industrial and technological applications. Example of some applications include geothermal reservoirs, drying of porous solids, heat exchanger design, petroleum production, filtration, chemical catalytic reactor, nuclear waste repositories, and geophysical flows. The prediction and knowledge of heat transfer rate and temperature distribution from a heated horizontal surface to surrounding ground water in a subsurface environment has important applications in the assessment of geothermal resources and the design of a geothermal power plant.

Keywords: *nusselt number (\bar{Nu}), rayleigh number (Ra), cone angle (C_A), radius ratio (R_r) and power law exponent (λ).*

GJSFR-A Classification : FOR Code: 090607



Strictly as per the compliance and regulations of :



Effect of Power Law Temperature Variation on a Vertical Conical Annular Porous Medium

Dr. D. Prabhakar ^α & Dr. G. Prabhakararao ^σ

Abstract- In this chapter, we concentrate on the study of heat transfer by natural convection in a saturated porous medium with a power law temperature variation on a vertical conical annular porous medium". In this study Finite Element Method (FEM) has been used to solve the governing partial differential equations. There have been considerable interest in studying natural or buoyancy – induced flows in fluid saturated porous media adjacent to surfaces in recent years. This interest stems from numerous possible industrial and technological applications. Example of some applications include geothermal reservoirs, drying of porous solids, heat exchanger design, petroleum production, filtration, chemical catalytic reactor, nuclear waste repositories, and geophysical flows. The prediction and knowledge of heat transfer rate and temperature distribution from a heated horizontal surface to surrounding ground water in a subsurface environment has important applications in the assessment of geothermal resources and the design of a geothermal power plant.

Keywords: nusselt number (Nu), rayleigh number (Ra), cone angle (C_A), radius ratio (R), and power law exponent (λ).

1. INTRODUCTION

There have been considerable interest in studying natural or buoyancy – induced flows in fluid saturated porous media adjacent to surfaces in recent years. This interest stems from numerous possible industrial and technological applications. Example of some applications include geothermal reservoirs, drying of porous solids, heat exchanger design, petroleum production, filtration, chemical catalytic reactor, nuclear waste repositories, and geophysical flows. The prediction and knowledge of heat transfer rate and temperature distribution from a heated horizontal surface to surrounding ground water in a subsurface environment has important applications in the assessment of geothermal resources and the design of a geothermal power plant. Ali J. Chamaka [1] have studied, laminar buoyancy – induced flow of a power – law fluid over a semi-infinite horizontal surface embedded in a uniform porous medium. Cheng and Chang [2] have used a similarity transformation in solving free convection flow from a horizontal surfaces in porous media while Nakayama and Koyama [3] have

employed the Karman – Pohlhausen approximate integral method. Chamkha [4] have considered free convection from a cone and a wedge in porous media.

In spite of the frequent occurrence of industrial applications using power-law fluids such as fossil fuels, molten plastics, polymer solutions, dyes, varnishes, suspensions, paints, and multi-grade oil, there have been little work done on power – law flows in porous media. Some of this work can be found in the papers by Chen and Chen [5,6] have obtained solutions for free convection power-law fluid flows over a vertical plate, horizontal circular cylinder, and a sphere embedded in a porous medium. Nakayama and Koyama [7] have generalized the work of Chen and Chen [5,6] to non-isothermal bodies of arbitrary shape. Chamkha [8,9] have considered steady and transient power-law fluid flow in a porous medium channel. Metha and Rao [10] have studied buoyancy-induced flow of power-law fluids over a nonisothermal horizontal plate embedded in a porous medium using a similarity transformation.

Hering and Grosh [11] examined the laminar natural convection flow over a non-isothermal cone. Cheng et al [12] studied the heat transfer of a Darcian fluid by natural convection over a cone. Gorla et al [13] studied the free convection of powerlaw fluid over the vertical frustum of a cone.

Natural convection about an impermeable vertical flat plate, horizontal plate, vertical cylinder, and vertical cone is studied by Cheng and Minkowycz [14], and Minkowycz and Cheng [15] respectively. studies of uniform surface mass transfer effect have been presented by Minkowycz and Cheng [16] for a vertical flat plate, Minkowycz et al. [17] for horizontal plate, Huang and Chen [18] for vertical Cylinder and Yih [19] for a vertical cone. Previous researches [14-19], however, have been only concentrated upon the power-law fluid. A number of industrially important fluids, including fossil fuels which can have saturated underground beds, display the behavior of power-law fluids, exhibit a non-linear relationship between shear strain rate and shear stress.

In this chapter, we concentrate on the study of heat transfer by natural convection in a saturated porous medium with a power law temperature variation on a vertical conical annular porous medium". In this study Finite Element Method (FEM) has been used to solve the governing partial differential equations. Results are presented interms of average Nusselt number (\bar{Nu}),

Author ^α : Sub Inspector of Police Department of fire Office, Yemmiganuru, Kurnool –District Andhra Pradesh, India. e-mail: dprabhakar1234@gmail.com

Author ^σ : Lecturer in Mathematics Department of Mathematics, S.V.G.M. Government Degree College, Kalyandurg, Anantapur-District, Andhra Pradesh, India. e-mail: nari.prabhu@gmail.com

streamlines and isothermal lines for various values of Rayleigh number (Ra), Cone angle (CA), Radius ratio (Rr) and power law exponent (l).

II. MATHEMATICAL FORMULATION

A vertical annular cone of inner radius r_i and outer radius r_0 as depicted by schematic diagram as shown in figure (A) is considered to investigate the heat transfer behavior. The co-ordinate system is chosen such that the r -axis points towards the width and z -axis towards the height of the cone respectively. Because of the annular nature, two important parameters emerge which are Cone angle (C_A) and Radius ratio (R_r) of the annulus. They are defined as

$$C_A = \frac{H_t}{r_0 - r_i}, \quad R_r = \frac{r_0 - r_i}{r_i}$$

where H_t is the height of the cone.

The inner surface of the cone is assumed to be power law functions and it varies in the vertical direction along the height of the inner wall of the vertical annular cone $T_h = T_\infty + B(z)\lambda$ and the outer surface at an ambient temperature T_∞ respectively. Where λ and B are the constants responsible for temperature variations along the length of the vertical annular cone.

We assume that the flow inside the porous medium is assumed to obey Darcy law and there is no phase change of fluid. The porous medium is saturated with fluid, the convective fluid and the porous medium are every where in local thermal equilibrium in the domain. The properties of the fluid and of the porous medium are homogeneous, isotropic constant except variation of fluid density with temperature. Under these assumptions the equations governing the flow, heat transfer are given by Continuity Equation:

$$\frac{\partial(ru)}{\partial r} + \frac{\partial(rw)}{\partial z} = 0 \quad (4.2.1)$$

The corresponding dimensional boundary conditions are

$$\text{at } r = r_i, \quad T_w = T_\infty \quad (4.2.10a)$$

$$r = r_0, \quad T = T_\infty, \quad u = 0 \quad (4.2.10b)$$

The new parameters arising due to cylindrical co-ordinates system are

$$\text{Non-dimensional Radius} \quad \bar{r} = \frac{r}{L} \quad (4.2.11a)$$

$$\text{Non-dimensional Height} \quad \bar{z} = \frac{z}{L} \quad (4.2.11b)$$

The velocity in r and z directions can be described by Darcy law as

Velocity in horizontal direction

$$u = \frac{-K}{\mu} \frac{\partial p}{\partial r} \quad (4.2.2)$$

velocity in vertical direction

$$w = \frac{-K}{\mu} \left(\frac{\partial p}{\partial z} + \rho g \right) \quad (4.2.3)$$

the permeability K of porous medium can be expressed as Bejan [27]

$$K = \frac{D_p^2 \phi^3}{180(1-\phi)^2} \quad (4.2.4)$$

The variation of density with respect to temperature can be described by Boussinesq approximation as

$$\rho = \rho_\infty [1 - \beta_T (T - T_\infty)] \quad (4.2.5)$$

Momentum Equation :

$$\frac{\partial w}{\partial r} - \frac{\partial u}{\partial z} = \frac{gK\beta}{\nu} \frac{\partial T}{\partial r} \quad (4.2.6)$$

Every equation:

$$u \frac{\partial T}{\partial r} + w \frac{\partial T}{\partial z} = \alpha \left(\frac{1}{r} \frac{\partial}{\partial r} \left(r \frac{\partial T}{\partial r} \right) + \frac{\partial^2 T}{\partial z^2} \right) \quad (4.2.7)$$

The continuity equation (4.2.1) can be satisfied by introducing the stream function ψ as

$$u = -\frac{1}{r} \frac{\partial \psi}{\partial z} \quad (4.2.8)$$

$$w = \frac{\partial \psi}{r \partial r} \quad (4.2.9)$$

$$\text{Non-dimensional stream function} \quad \bar{\psi} = \frac{\psi}{\alpha L} \quad (4.2.11c)$$

$$\text{Non-dimensional Temperature} \quad \bar{T} = \frac{(T - T_\infty)}{(T_w - T_\infty)} \quad (4.2.11d)$$

$$\text{Rayleigh number} \quad Ra = \frac{g\beta_T \Delta T K L}{\nu \alpha} \quad (4.2.11e)$$

The non-dimensional equations for the heat transfer in vertical cone are

$$\text{Momentum equation:} \quad \frac{\partial^2 \bar{\psi}}{\partial \bar{z}^2} + \bar{r} \left(\frac{1}{\bar{r}} \frac{\partial \bar{\psi}}{\partial \bar{r}} \right) = \bar{r} Ra \frac{\partial \bar{T}}{\partial \bar{r}} \quad (4.2.12)$$

$$\text{Energy equation :} \quad \frac{1}{\bar{r}} \left[\frac{\partial \bar{\psi}}{\partial \bar{r}} \frac{\partial \bar{T}}{\partial \bar{z}} - \frac{\partial \bar{\psi}}{\partial \bar{z}} \frac{\partial \bar{T}}{\partial \bar{r}} \right] = \left(\frac{1}{\bar{r}} \frac{\partial}{\partial \bar{r}} \left(\bar{r} \frac{\partial \bar{T}}{\partial \bar{r}} \right) + \frac{\partial^2 \bar{T}}{\partial \bar{z}^2} \right) \quad (4.2.13)$$

III. SOLUTION OF THE GOVERNING EQUATIONS

Applying Galerkin method to momentum equation (4.2.12) yields:

$$\{R^e\} = - \int_V N^T \left(\frac{\partial^2 \bar{\psi}}{\partial \bar{z}^2} + \bar{r} \frac{\partial}{\partial \bar{r}} \left(\frac{1}{\bar{r}} \frac{\partial \bar{\psi}}{\partial \bar{r}} \right) - \bar{r} Ra \frac{\partial \bar{T}}{\partial \bar{r}} \right) dV \quad (4.3.1)$$

$$\{R^e\} = - \int_A N^T \left(\frac{\partial^2 \bar{\psi}}{\partial \bar{z}^2} + \bar{r} \frac{\partial}{\partial \bar{r}} \left(\frac{1}{\bar{r}} \frac{\partial \bar{\psi}}{\partial \bar{r}} \right) - \bar{r} Ra \frac{\partial \bar{T}}{\partial \bar{r}} \right) 2\bar{\Pi} \bar{r} dA \quad (4.3.2)$$

Where R^e is the residue. Considering individual terms of equation (4.3.2)
The differentiation of following term results into

$$\frac{\partial}{\partial \bar{r}} \left[[N^T] \frac{\partial \bar{\psi}}{\partial \bar{r}} \right] = [N^T] \frac{\partial^2 \bar{\psi}}{\partial \bar{r}^2} + \frac{\partial [N^T]}{\partial \bar{r}} \frac{\partial \bar{\psi}}{\partial \bar{r}} \quad (4.3.3)$$

Thus

$$\int_A N^T \frac{\partial^2 \bar{\psi}}{\partial \bar{r}^2} dA = \int_A \frac{\partial}{\partial \bar{r}} \left([N^T] \frac{\partial^2 \bar{\psi}}{\partial \bar{r}^2} \right) 2\bar{\Pi} \bar{r} dA - \int_A \frac{\partial [N^T]}{\partial \bar{r}} \frac{\partial \bar{\psi}}{\partial \bar{r}} \quad (4.3.4)$$

The first term on right hand side of equation (4.3.4) can be transformed into surface integral by the application of Greens theorem and leads to inter-element requirement at boundaries of an element. The boundary conditions are incorporated in the force vector.

Let us consider that the variable to be determined in the triangular area as "T". The polynomial function for "T" can be expressed as

$$\mathbf{T} = \alpha_1 + \alpha_2 \mathbf{r} + \alpha_3 \quad (4.3.5)$$

The variable T has the value T_i , T_j & T_k at the nodal position i , j and k of the element. The r and z coordinates at these points are r_i , r_j , r_k and z_i , z_j , z_k respectively.

$$\text{Since} \quad T = N_i T_i + N_j T_j + N_k T_k \quad (4.3.6)$$

Where N_i , N_j & N_k are shape functions given by

$$N_m = \frac{a_m + b_m r + c_m z}{2A} \quad (4.3.7)$$

Making use of (4.3.7) gives

$$\int_A N^T \frac{\partial^2 \bar{T}}{\partial z^2} 2\Pi r dA = - \int_A \frac{\partial N^T}{\partial r} \frac{\partial N}{\partial r} \begin{Bmatrix} \bar{\psi}_1 \\ \bar{\psi}_2 \\ \bar{\psi}_3 \end{Bmatrix} dA \quad (4.3.8)$$

Substitution of (4.3.7) into (4.3.8) gives:

$$\begin{aligned} &= \frac{-1}{(2A)^2} \int_A \begin{bmatrix} b_1 \\ b_2 \\ b_3 \end{bmatrix} [b_1 b_2 b_3] \begin{Bmatrix} \bar{\psi}_1 \\ \bar{\psi}_2 \\ \bar{\psi}_3 \end{Bmatrix} 2\Pi r dA \\ &= -\frac{2\Pi \bar{R}}{4A} \begin{bmatrix} b_1^2 & b_1 b_2 & b_1 b_3 \\ b_1 b_2 & b_2^2 & b_2 b_3 \\ b_1 b_3 & b_2 b_3 & b_3^2 \end{bmatrix} \begin{Bmatrix} \bar{\psi}_1 \\ \bar{\psi}_2 \\ \bar{\psi}_3 \end{Bmatrix} \end{aligned} \quad (4.3.9)$$

Similarly

$$\int_A N^T \frac{\partial^2 \bar{\psi}}{\partial z^2} 2\Pi r dA = -\frac{2\Pi \bar{R}}{4A} \begin{bmatrix} c_1^2 & c_1 c_2 & c_1 c_3 \\ c_1 c_2 & c_2^2 & c_2 c_3 \\ c_1 c_3 & c_2 c_3 & c_3^2 \end{bmatrix} \begin{Bmatrix} \bar{\psi}_1 \\ \bar{\psi}_2 \\ \bar{\psi}_3 \end{Bmatrix} \quad (4.3.10)$$

The third term of equation (4.3.2) is

$$\int_A N^T r Ra \frac{\partial \bar{T}}{\partial r} 2\Pi r dA = Ra \int_A N^T r \frac{\partial \bar{T}}{\partial r} 2\Pi r dA \quad (4.3.11)$$

Since

$$M_1 = N_1, \quad M_2 = N_2, \quad M_3 = N_3$$

Where M_1 , M_2 , and M_3 are the area ratios of the triangle and N_1 , N_2 and N_3 are the shape functions.

Replacing the shape functions in the above equation (4.3.11) gives

$$\int_A N^T r Ra \frac{\partial \bar{T}}{\partial r} 2\Pi r dA = r Ra \int_A \begin{bmatrix} M_1 \\ M_2 \\ M_3 \end{bmatrix} \frac{\partial [N]}{\partial r} \begin{bmatrix} \bar{T}_1 \\ \bar{T}_2 \\ \bar{T}_3 \end{bmatrix} 2\Pi r dA \quad (4.3.12)$$

$$\begin{aligned} &= Ra \frac{A}{3} \begin{bmatrix} 1 \\ 1 \\ 1 \end{bmatrix} \frac{2\Pi \bar{R}^2}{2A} [b_1 + b_2 + b_3] \begin{bmatrix} \bar{T}_1 \\ \bar{T}_2 \\ \bar{T}_3 \end{bmatrix} \\ &= \frac{2\Pi \bar{R}^2 Ra}{6} \begin{Bmatrix} b_1 \bar{T}_1 + b_2 \bar{T}_2 + b_3 \bar{T}_3 \\ b_1 \bar{T}_1 + b_2 \bar{T}_2 + b_3 \bar{T}_3 \\ b_1 \bar{T}_1 + b_2 \bar{T}_2 + b_3 \bar{T}_3 \end{Bmatrix} \end{aligned} \quad (4.3.13)$$

Now Momentum equation leads to

$$\frac{2\Pi \bar{R}}{4A} \begin{bmatrix} b^2 & b_1 b_2 & b_1 b_3 \\ b_1 b_2 & b_2^2 & b_2 b_3 \\ b_1 b_3 & b_2 b_3 & b_3^2 \end{bmatrix} + \begin{bmatrix} c_1^2 & c_1 c_2 & c_1 c_3 \\ c_1 c_2 & c_2^2 & c_2 c_3 \\ c_1 c_3 & c_2 c_3 & c_3^2 \end{bmatrix} \begin{Bmatrix} \bar{\psi}_1 \\ \bar{\psi}_2 \\ \bar{\psi}_3 \end{Bmatrix} + \frac{2\Pi \bar{R}^2 Ra}{6} \begin{Bmatrix} b_1 \bar{T}_1 + b_2 \bar{T}_2 + b_3 \bar{T}_3 \\ b_1 \bar{T}_1 + b_2 \bar{T}_2 + b_3 \bar{T}_3 \\ b_1 \bar{T}_1 + b_2 \bar{T}_2 + b_3 \bar{T}_3 \end{Bmatrix} = 0 \quad (4.3.14)$$

Which is in the form of the stiffness matrix

$$[K_s] \{ \bar{\psi} \} = \{ f \} \quad (4.3.15)$$

Similarly application of Galerking method to Energy equation gives

$$\{ R^e \} = - \int_A N^T \left[\frac{1}{r} \left(\frac{\partial \bar{\psi}}{\partial r} \frac{\partial \bar{T}}{\partial z} - \frac{\partial \bar{\psi}}{\partial z} \frac{\partial \bar{T}}{\partial r} \right) \right] - \left[\frac{1}{r} \frac{\partial}{\partial r} \left(r \frac{\partial \bar{T}}{\partial r} \right) + \frac{\partial^2 \bar{T}}{\partial z^2} \right] 2\pi r dA \quad (4.3.16)$$

Considering the terms individually of the above equation (4.3.16)

$$\int_A [N]^T \frac{\partial \bar{\psi}}{\partial z} \frac{\partial \bar{T}}{\partial r} 2\pi r dA = \int_A \begin{bmatrix} M_1 \\ M_2 \\ M_3 \end{bmatrix} \frac{\partial [N]}{\partial z} \{ \bar{\psi} \} \frac{\partial [N]}{\partial r} \{ \bar{T} \} 2\pi r dA \quad (4.3.17)$$

$$= \frac{2\pi A}{3} X \frac{1}{4A^2} [c_1 \bar{\psi}_1 + c_2 \bar{\psi}_2 + c_3 \bar{\psi}_3] [b_1, b_2, b_3] \begin{Bmatrix} \bar{T}_1 \\ \bar{T}_2 \\ \bar{T}_3 \end{Bmatrix}$$

$$= \frac{2\pi}{12A} \begin{Bmatrix} c_1 \bar{\psi}_1 + c_2 \bar{\psi}_2 + c_3 \bar{\psi}_3 \\ c_1 \bar{\psi}_1 + c_2 \bar{\psi}_2 + c_3 \bar{\psi}_3 \\ c_1 \bar{\psi}_1 + c_2 \bar{\psi}_2 + c_3 \bar{\psi}_3 \end{Bmatrix} [b_1, b_2, b_3] \begin{Bmatrix} \bar{T}_1 \\ \bar{T}_2 \\ \bar{T}_3 \end{Bmatrix} \quad (4.3.18)$$

Following the same above steps

$$\int_A [N]^T \frac{\partial \bar{\psi}}{\partial r} \frac{\partial \bar{T}}{\partial z} 2\pi r dA = \int_A \begin{bmatrix} M_1 \\ M_2 \\ M_3 \end{bmatrix} \frac{\partial [N]}{\partial r} \{ \bar{\psi} \} \frac{\partial [N]}{\partial z} \{ \bar{T} \} 2\pi r dA \quad (4.3.19)$$

$$\int_A N^T \frac{\partial \bar{\psi}}{\partial r} \frac{\partial \bar{T}}{\partial z} 2\pi r dA = \frac{2\pi}{12A} \begin{Bmatrix} b_1 \bar{\psi}_1 + b_2 \bar{\psi}_2 + b_3 \bar{\psi}_3 \\ b_1 \bar{\psi}_1 + b_2 \bar{\psi}_2 + b_3 \bar{\psi}_3 \\ b_1 \bar{\psi}_1 + b_2 \bar{\psi}_2 + b_3 \bar{\psi}_3 \end{Bmatrix} [c_1, c_2, c_3] \begin{Bmatrix} \bar{T}_1 \\ \bar{T}_2 \\ \bar{T}_3 \end{Bmatrix} \quad (4.3.20)$$

The remaining terms of Energy equation can be evaluated in similar fashion of equation (4.3.16)

$$\int_A N^T \frac{1}{r} \frac{\partial}{\partial r} \left(r \frac{\partial \bar{T}}{\partial r} \right) 2\pi r dA = - \frac{2\pi R}{4A} \begin{bmatrix} b_1^2 & b_1 b_2 & b_1 b_3 \\ b_1 b_2 & b_2^2 & b_2 b_3 \\ b_1 b_3 & b_2 b_3 & b_3^2 \end{bmatrix} \begin{Bmatrix} \bar{T}_1 \\ \bar{T}_2 \\ \bar{T}_3 \end{Bmatrix} \quad (4.3.21)$$

$$\int_A N^T \frac{\partial^2 \bar{T}}{\partial z^2} 2\pi r dA = - \frac{2\pi R}{4A} \begin{bmatrix} c_1^2 & c_1 c_2 & c_1 c_3 \\ c_1 c_2 & c_2^2 & c_2 c_3 \\ c_1 c_3 & c_2 c_3 & c_3^2 \end{bmatrix} \begin{Bmatrix} \bar{T}_1 \\ \bar{T}_2 \\ \bar{T}_3 \end{Bmatrix} \quad (4.3.22)$$

Thus the stiffness matrix of Energy equation is given by

$$\left[\frac{2\Pi}{12A} \begin{Bmatrix} c_1\bar{\psi}_1 + c_2\bar{\psi}_2 + c_3\bar{\psi}_3 \\ c_1\bar{\psi}_1 + c_2\bar{\psi}_2 + c_3\bar{\psi}_3 \\ c_1\bar{\psi}_1 + c_2\bar{\psi}_2 + c_3\bar{\psi}_3 \end{Bmatrix} [b_1, b_2, b_3] - \frac{2\Pi}{12A} \begin{Bmatrix} b_1\bar{\psi}_1 + b_2\bar{\psi}_2 + b_3\bar{\psi}_3 \\ b_1\bar{\psi}_1 + b_2\bar{\psi}_2 + b_3\bar{\psi}_3 \\ b_1\bar{\psi}_1 + b_2\bar{\psi}_2 + b_3\bar{\psi}_3 \end{Bmatrix} [c_1, c_2, c_3] \right] \begin{Bmatrix} \bar{T}_1 \\ \bar{T}_2 \\ \bar{T}_3 \end{Bmatrix} + \frac{2\Pi R}{4A} \begin{Bmatrix} b_1^2 & b_1 b_2 & b_1 b_3 \\ b_1 b_2 & b_2^2 & b_2 b_3 \\ b_1 b_3 & b_2 b_3 & b_3^2 \end{Bmatrix} \begin{Bmatrix} \bar{T}_1 \\ \bar{T}_2 \\ \bar{T}_3 \end{Bmatrix} + \begin{Bmatrix} c_1^2 & c_1 c_2 & c_1 c_3 \\ c_1 c_2 & c_2^2 & c_2 c_3 \\ c_1 c_2 & c_2 c_3 & c_3^2 \end{Bmatrix} \begin{Bmatrix} \bar{T}_1 \\ \bar{T}_2 \\ \bar{T}_3 \end{Bmatrix} = 0 \quad (4.3.23)$$

IV. RESULTS AND DISCUSSION

The average Nusselt number (\bar{Nu}), is given by

Results are obtained in terms of the average Nusselt number (\bar{Nu}) at hot wall for various parameters such as Rayleigh number (Ra), Radius ratio (R_r), Cone angle (C_A) and Power law exponent (λ) when heat supplied to the vertical annular cone.

$$\bar{Nu} = \int_0^1 \left(\frac{\partial \bar{T}}{\partial r} \right)$$

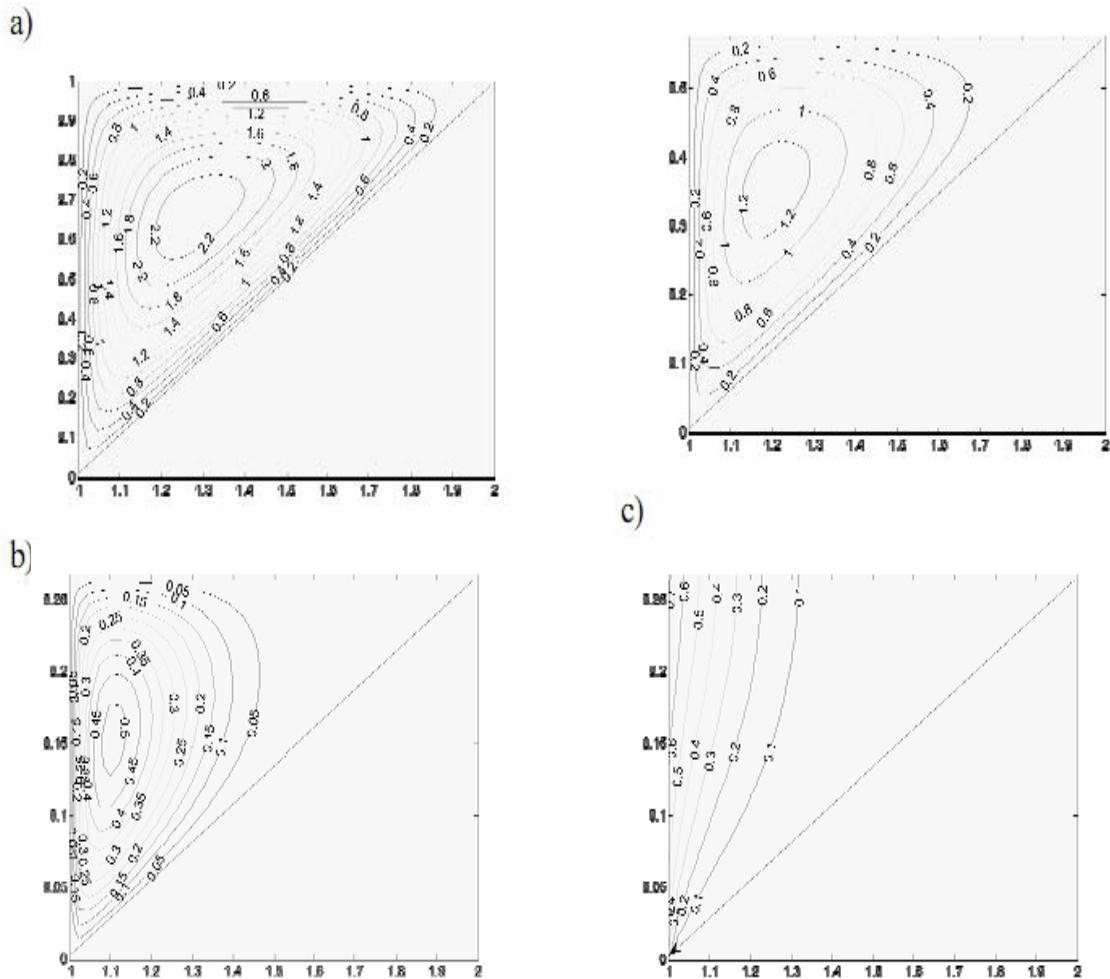


Figure 4.4.1 : Streamlines(left) and Isotherms(Right) for $Ra=50, R_r=1, \lambda=0.25$
 a) $C_A = 45$ b) $C_A = 60$ c) $C_A = 75$

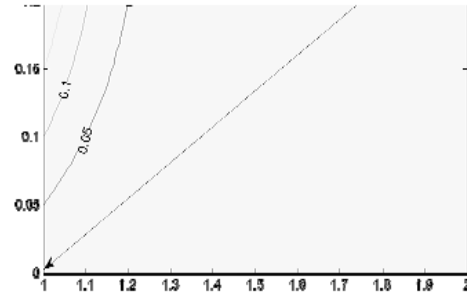
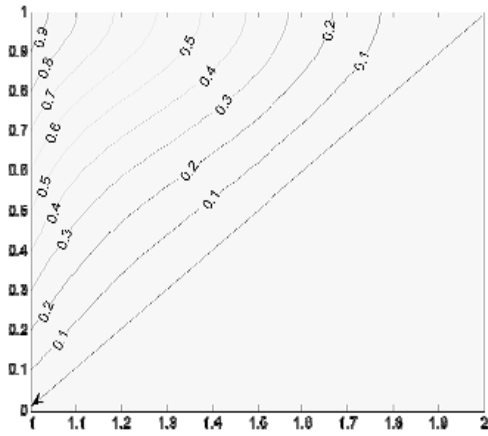


Fig (4.4.1) shows the streamlines and isothermal lines distribution inside the porous medium of the vertical annular cone for various values of Cone angle (C_A) at $Ra = 50$, $R_r = 1$, $\lambda = 0.25$. The streamlines and isothermal lines move away from the cold wall and reach nearer to hot wall as Cone angle (C_A) increases. It can be seen that the thermal boundary layer thickness decreases as cone angle (C_A) increases. It is obvious from the Fig (4.4.1) that the heat transfer rate is higher at the centre portion of the annular cone at higher values of Cone angle (C_A), which is indicated by crowding of isothermal lines in the vicinity of centre portion of hot wall as shown in figure.

Fig (4.4.2) depicts the streamlines and isothermal lines inside porous medium for various values of Cone angle (C_A) at $Ra = 50$, $R_r = 1$ and $\lambda = 1$ when compared with Fig (4.4.1) by Fig (4.4.2) formation of streamlines and isothermal lines decreases the occupation of the domain for the increased values of Cone angle (C_A). This is due to reason that the increase of Power law index ($\lambda = 1$).

vertical annular cone for various values of Cone angle (C_A) at $R_r = 1$, $\lambda = 1$. It is found that the average Nusselt number (\bar{Nu}) increases with increase in Rayleigh number (Ra). It can be seen that the average Nusselt number (\bar{Nu}) increases with increase in Cone angle (C_A). For a given Rayleigh number (Ra), the difference between two different values of Cone angle (C_A) increase with increase in Cone angle (C_A). For instance, the average Nusselt number (\bar{Nu}) increases by 25%, when Cone angle (C_A) is increased from 45 to 60 at $Ra = 10$. However the average Nusselt number (\bar{Nu}) increased by 45%. When Cone angle (C_A) is increased 45 to 60 at $Ra = 100$. This difference becomes more prominent as the Rayleigh number (Ra) increase.

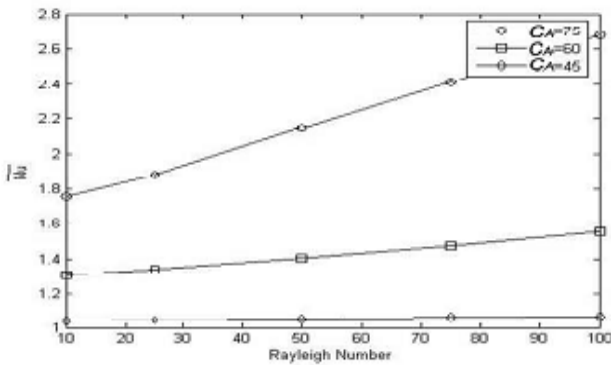


Fig.4.4.3: Nu variations with Ra at hot surface for different values of C_A at $R_r=1$, $\lambda = 1$ Fig (4.4.3) illustrates the variation of average Nusselt number (\bar{Nu}) at hot wall, with respect to Rayleigh number (Ra) of the

a)

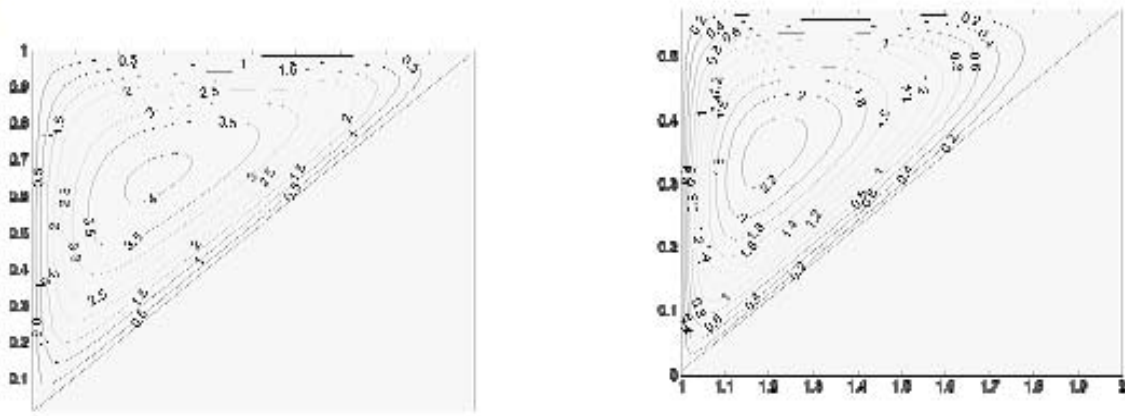


Figure 4.4.4 : Streamlines(left) and Isotherms(Right) for $Ra=100, R_r=1, \lambda=0.25$
 a) $C_A = 45$ b) $C_A = 60$ c) $C_A = 75$

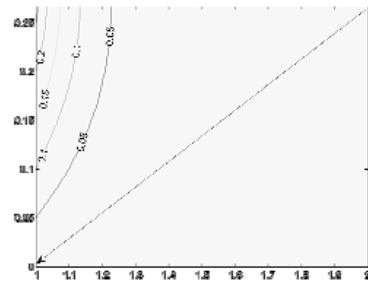
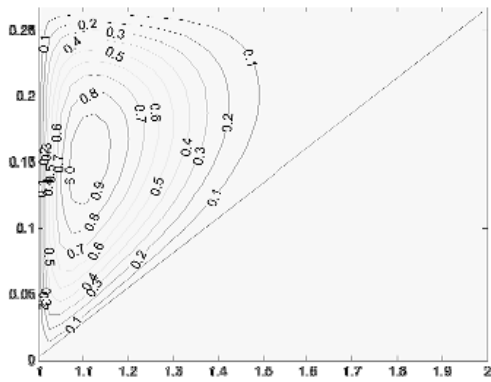
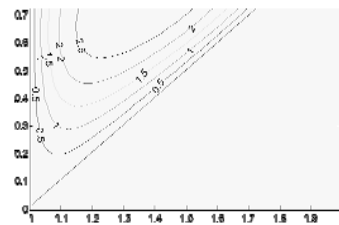
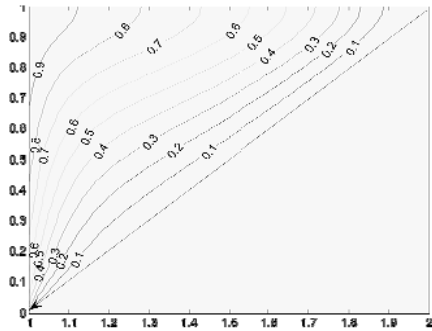
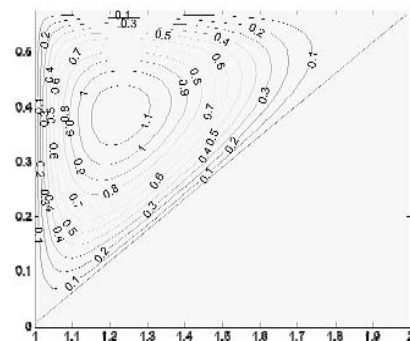
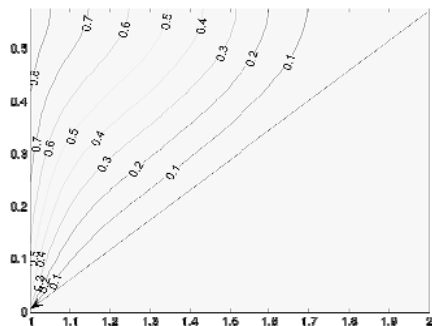


Figure 4.4.5 : Streamlines(left) and Isotherms Isotherms (Right) for $Ra=100, R_r=1, \lambda = 1$
 a) $C_A = 45$ b) $C_A = 60$ c) $C_A = 75$



b)



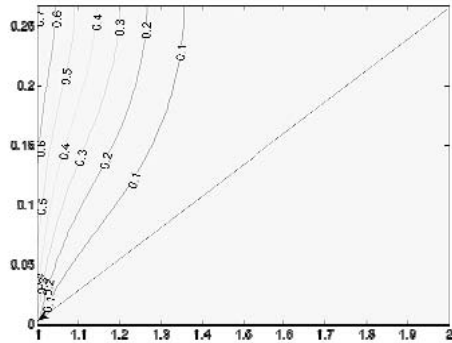


Fig (4.4.4) illustrates the streamlines and isothermal lines distribution inside the porous medium for various values of Cone angle (C_A) at $Ra = 100$, $R_r = 1$ and $\lambda = 0.25$. The boundary layer thickness moves from colar wall to Hot wall in the occupation of the domain by stream and isothermal lines decreases for the increased values of Cone angles ($C_A = 45, 60, 75$), i.e. boundary layer thickness reduces with increase in Cone angle (C_A).

Fig (4.4.5) shows the streamlines and isothermal lines inside the porous medium for various values of Cone angle (C_A) at $Ra = 100$, $R_r = 1$ and $\lambda = 1$. When compared with the Fig (4.4.2) by Fig (4.4.5) the formation of the fluid by the stream and isothermal lines decreased and occupies the domain by stream and isothermal lines decreased. This is due to the increased values of power law index ($\lambda = 1$)

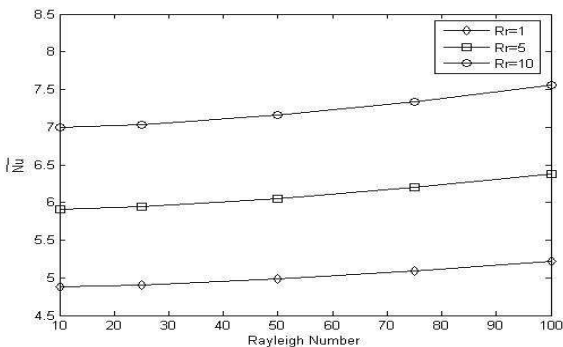


Figure 4.4.6 : \bar{Nu} variations with Ra at hot surface for different values of R_r at $C_A=75$, $\lambda=0.25$

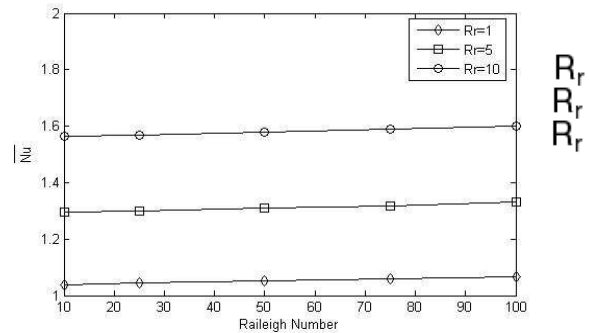
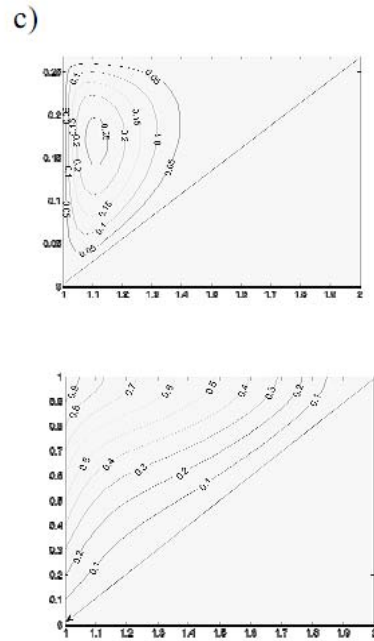


Figure 4.4.7 : \bar{Nu} variations with Ra at hot surface for different values of R_r at $C_A=75$, $\lambda=1$

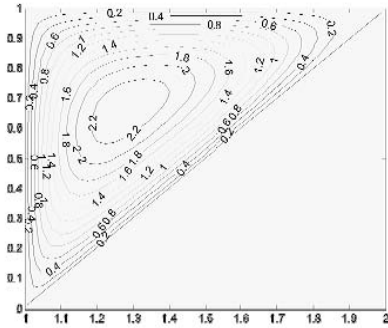
Fig (4.4.6) illustrates the variation of average Nusselt number (\bar{Nu}) at hot wall, with respect to Rayleigh number (Ra) of vertical annular cone for various values of Radius ratio (R_r) at $C_A = 75$, $\lambda = 0.25$. It is found that the average Nusselt number (\bar{Nu}) increases with increase in Rayleigh number (Ra). It can be seen that the average Nusselt number (\bar{Nu}) increases with increase in Radius ratio (R_r). For a given Rayleigh number (Ra), the difference between the average Radius ratio (R_r) at two different values of Radius ratio (R_r). For instance, the average Nusselt number (\bar{Nu}) increased by 22% when Radius ratio (R_r) is increased from 1 to 5, at $Ra = 10$. However the average Nusselt number (\bar{Nu}) increased by 21%, when Radius ratio (R_r) is increased from 1 to 5 at $Ra = 100$. This shows that the average Nusselt number (\bar{Nu}) increases linearly with the increase in Rayleigh number (Ra).

Fig (4.4.7) demonstrates the effect of Rayleigh number (Ra) on the average Nusselt number (\bar{Nu}) for various values of Radius ratio (R_r). This figure is obtained for $CA=75$, $\lambda = 1$. It is found that the average Nusselt number (Nu) increases slightly with increase in

Rayleigh number (Ra). It can be seen that the average Nusselt number (\bar{Nu}) increase with increase in Radius ratio (R_r). For a given Rayleigh number (Ra), the difference between the average Nusselt number (\bar{Nu}) at two different values of Radius ratio (R_r) increases with increase in Radius ratio (R_r). For instance, the average Nusselt number (\bar{Nu}) increased by 25% when Radius

ratio (R_r) is increased from 1 to 5 at $Ra = 10$. However the average Nusselt number (\bar{Nu}) increased by 23%, when Radius ratio (R_r) is increased from 1 to 5 at $Ra = 100$. This shows that the average Nusselt number (\bar{Nu}) increases linearly with the increase in Rayleigh number (Ra).

a)



b)

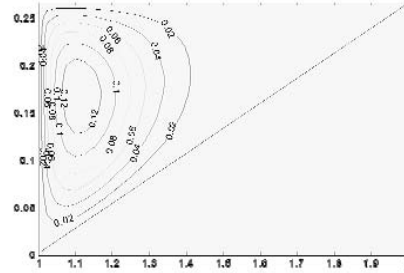
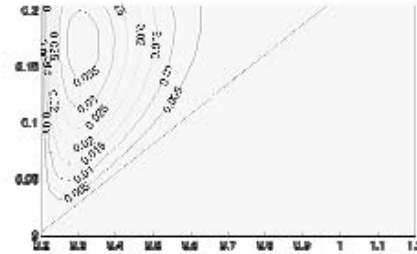
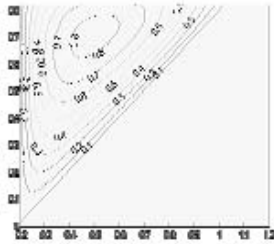
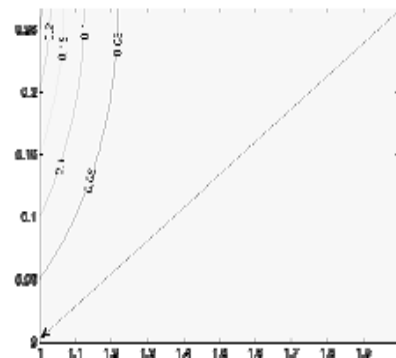
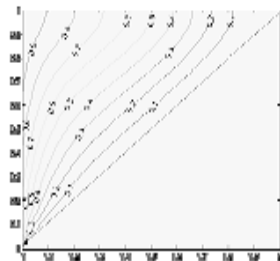
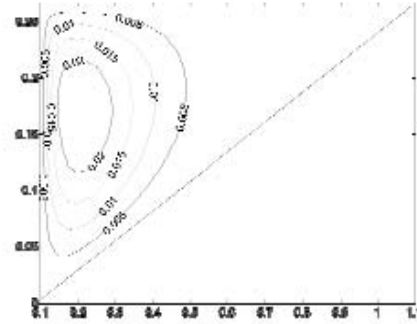
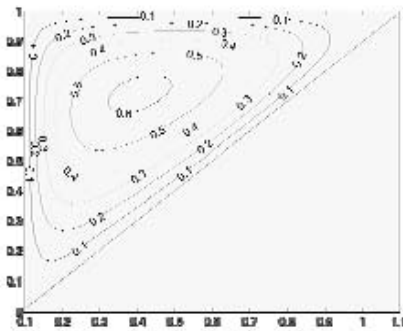


Figure 4.4.8 : Streamlines(left) and Isotherms(Right) $C_A = 45, \lambda = 0.25$
 a) $R_r=1$ b) $R_r=5$, c) $R_r=10$



c)



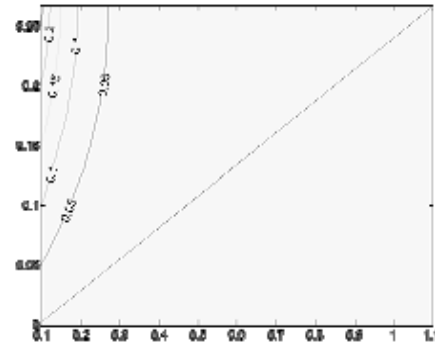
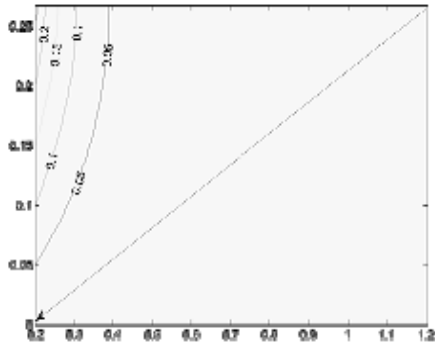


Fig (4.4.8) illustrates the streamlines and isothermal lines distribution inside the porous medium for various values of Radius ratio (R_r) at $Ra = 50$, $C_A = 45$ and $\lambda=0.25$. The magnitude of streamlines decreases as the Radius ratio (R_r) increases. This is due to the reason the increased Radius ratio (R_r) promotes the fluid movements due to higher buoyancy force, which in term allows the connection heat transfer to take dominant position. The increased Radius ratio (R_r) particularly enhance the heat transfer rate at lower portion of hot and cold walls of vertical annular cone respectively. The fluid circulation moves towards the lower portion of cold wall when Radius ratio (R_r) is increased.

Fig (4.4.9) shows the streamlines and isothermal lines inside the porous medium for various values of Radius ratio (R_r) at $Ra = 50$, $CA = 75$, and $\lambda=1$. The boundary layer thickness decreases when Radius ratio (R_r) increases and also occupies the half of the domain by stream lines. Where as for the same Radius ratio (R_r) values of isothermal lines remain same.

can be seen that the average Nusselt number (\bar{Nu}) decreases with increase in Power law exponent (λ). For a given Rayleigh number (Ra) the difference between the average Nusselt number (\bar{Nu}) at different values of power law exponent (λ) decreases with increase in power law exponent (λ). For instance, the average Nusselt number (\bar{Nu}) decreased by 70%, when power law exponent (λ) is increased from 0 to 1 at $Ra = 10$. However the average Nusselt number (\bar{Nu}) decreased by 71.2%, when power law exponent (λ) is increased from 0 to 1 at $Ra = 100$. This shows that the average Nusselt number (\bar{Nu}) increases with the increase in Rayleigh number (Ra) for $\lambda = 0$ and increases as λ increases.

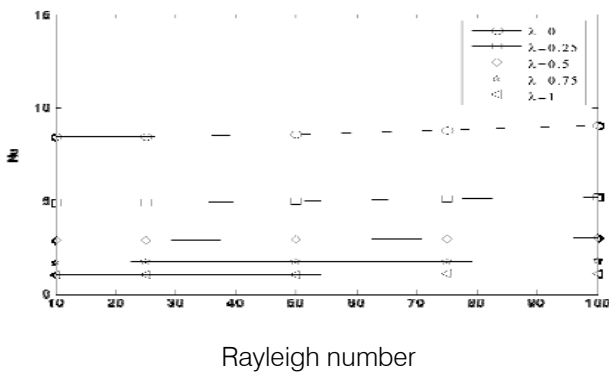


Figure 4.4.10 : Nu variations with Ra at hot surface for different values of λ at $C_A=75$, $R_r=1$

Fig (4.4.10) illustrates the variation of average Nusselt number (\bar{Nu}) at hot wall, with respect to Rayleigh number (Ra) of the vertical annular cone for various values of power law exponent (λ) at $C_A = 75$, $R_r = 1$. It is found that the average Nusselt number (\bar{Nu}) increases with the increase in Rayleigh number (Ra). It

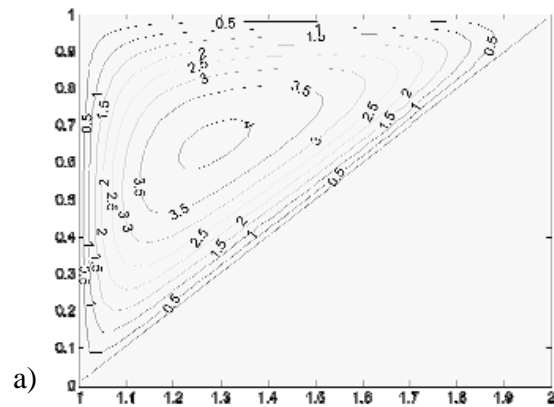
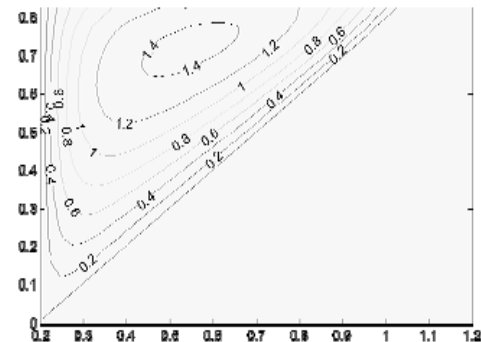


Figure 4.4.11 : Streamlines(left) and Isotherms(Right) for $Ra=100$, $C_A = 45$, $\lambda=0.25$ a) $R_r=1$ b) $R_r=5$, c) $R_r=10$



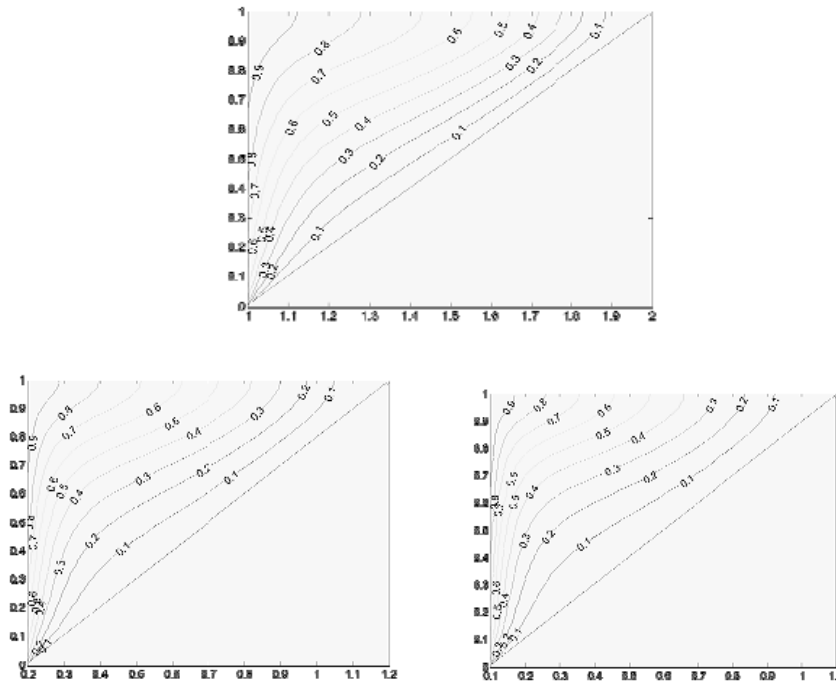


Figure 4.4.12 : Streamlines(left) and Isotherms(Right) for $Ra=100$, $C_A = 75$, $\lambda=1$
a) $R_r=1$ b) $R_r=5$ c) $R_r=10$

Fig (4.4.11) shows the streamlines and isothermal lines distribution inside the porous medium of the vertical annular cone for various values of Radius ratio (R_r) at $Ra = 100$, $C_A = 45$ and $l = 0.25$. The streamlines move away from the cold wall and reach nearer to hot wall as Radius ratio (R_r) increases. It can be seen that the thermal boundary layer thickness decreases as Radius ratio (R_r) increases and occupies the whole domain of cone, whereas isothermal lines for the same value of Radius ratio (R_r) remains same.

Fig (4.4.12) depicts the streamlines and isothermal lines inside the porous medium for various values of Radius ratio (R_r) at $Ra = 100$, $C_A = 75$ and $r = 1$. The stream lines move away from the cold wall and reach nearer to hot wall as Radius ratio (R_r) increases. It can be seen that the thermal boundary layer thickness decreases as Radius ratio (R_r) increases and occupying half of the domain of cone, whereas isothermal lines for the same value of Radius ratio (R_r) remains same.

REFERENCES RÉFÉRENCES REFERENCIAS

1. Ali J. Chamkha, Int. comm. Heat Mass Transfer – 24, p – 805 (1997).
2. P. Cheng and I.D. Chang, Int. J. Heat Mass Transfer – 19, p 1267 (1976).
3. A. Nakayama and H. Koyama, Appl. Sci. Res – 48, p – 55 (1991).
4. A.J. Chamkha, Int. comm. Heat and Mass Transfer – 23, p – 875 (1996).
5. H.T. Chen and C.K. Chen, J. Heat Transfer – 110, p – 257 (1988).

6. H.T. Chen and C.K. Chen, Int. comm. Heat and Mass Transfer – 15, p – 605 (1988).
7. A. Nakayama and H. Koyama, Heat fluid flow – 8, p – 240 (1987).
8. A.J. Chamkha fluid / particle separation J – 7, p – 4 (1994).
9. A.J. Chakha, fluid / particle separation J – 9, p – 129 (1996).
10. K.N. Metha and K.N. Rao, Int. J. Engineering. Sci – 32, p – 521 (1994).
11. R.G. Hering and R.J. Grosh, Int. J. Heat Mass Transfer – 5, p – 1059 (1962).
12. P. Cheng, T.T. Le and Pop, Int. comm. Heat Mass Transfer – 12, p – 705 (1985).
13. R.S.R. Gorla, V. Krishanan and I. Pop, Int. J. Engng. Sci. – 32, p – 1791 (1994).
14. P. Cheng and W.J. Minkowycz, J. Geophysics. Res – 82, p – 2040 (1977).
15. P. Cheng and W.J. Minkowycz, Int. J. Heat Mass Transfer – 19, p – 805 (1976).
16. W.J. Minkowycz and P. Cheng Lett. Heat Mass Transfer – 9, p – 159 (1982).
17. W.J. Minkowycz, P. Cheng and F. Moalem, Int. comm. Heat Mass Transfer – 12, p – 55 (1985).
18. M.J. Huang and C.K. Chen, ASME J. Energy Resources Technology – 107, p – 394 (1985).
19. K.A. Yih, Int. comm. Heat Mass Transfer – 24, p – 1195 (1997).